Published as:
Zawadzka, M.; Wang, J.; Blau, W. J.; Senge, M. O. (2013):
Modeling of Nonlinear Absorption of 5,10-A_2B_2 Porphyrins in the Nanosecond Regime.
The Journal of Physical Chemisty A **117**, 15–26.

Modeling of Nonlinear Absorption of 5,10-A_2B_2 Porphyrins in the Nanosecond Regime

Monika Zawadzka,[a] *Jun Wang,*[b] *Werner J. Blau*[c] *and Mathias O. Senge**[a]

[a] School of Chemistry, SFI Tetrapyrrole Laboratory, Trinity Biomedical Sciences Institute, 152-160 Pearse Street, Trinity College Dublin, Dublin 2, Ireland.

[b] Key Laboratory of Materials for High Power Lasers, Shanghai Institute of Optics and Fine Mechanics, Chinese Academy of Science, 201800, Shanghai, China

[c] School of Physics, Trinity College Dublin, Dublin 2, Ireland.

RECEIVED DATE (to be automatically inserted after your manuscript is accepted if required according to the journal that you are submitting your paper to)

*To whom correspondence should be addressed. E-mail: sengem@tcd.ie

The nonlinear absorption (NLA) properties of free base and metalated porphyrins with a unique 5,10-A_2B_2 substitution pattern were studied with open Z-scan technique at 532 nm in the nanosecond regime over a broad range of input fluence. The NLA responses were found to be dependent on structural features and the solvent used. In most cases the character of the response differed from that typically observed for other porphyrins under similar experimental conditions (*i.e.*, reverse saturable absorption, RSA), suggesting distinct photophysical properties. A series of models was considered in order to understand the NLA responses. Although the character of the responses varied between compounds and solvents it was found that one model fits best all of the recorded responses. Thus, a

four-level model with simultaneous two-photon absorption arising from the higher excited state is proposed (1+1+2 photon absorption).

KEYWORDS. Nonlinear optics, optical limiting, macrocyclic dyes, tetrapyrrole

Introduction

Nonlinear absorption (NLA) can be expressed phenomenally as an increase or decrease in transmission with intensity. Such behavior finds applications in Q-switching, mode locking and optical limiting. A more detailed understanding of the underlying mechanisms occurring in materials ranging from organic dyes, fullerenes to semiconductors is required for further practical advances in this area.[1-3]

Typically a five-level Jablonski model,[4] is used to explain the behavior of a material (here organic dyes) under illumination with light (Fig. 1). At resonant and close to resonant excitation wavelength NLA active materials exhibit a transmission drop through sequential absorption of photons, *i.e.* reverse saturable absorption (RSA), provided that the excited state absorption cross-section is higher than that of the ground state. Otherwise the opposite phenomenon, *i.e.* an increase in transmission with intensity – saturable absorption (SA) will be observed. The transmission drop can proceed as well through simultaneous absorption of photons – *e.g.*, multiphoton absorption processes such as two-photon absorption (TPA). Such k-photon absorptive processes arise at 1/k of the resonant frequency. Often the five-level model can be simplified when fitting NLA responses. Once subnanosecond pulses are used, intersystem crossing (ISC) from S_1 to T_1 can often be neglected since the lifetime of this transition is typically on the order of ns in organic dyes. Under ns pulses, provided that ISC is fast and efficient, absorption arising from S_1 is often ignored. Usually populations of higher excited states can be neglected since their lifetimes are very short (~ps or less).[5]

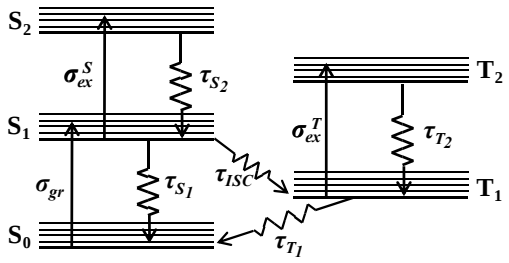

Figure 1: Five-level energy diagram. Solid lines represent absorption, jagged ones decay paths. S_0, S_1 and S_2 are singlet states, T_1, T_2 are triplet states. σ_{gr} stands for ground state absorption cross-section, σ_{ex}^{S} and σ_{ex}^{T} for singlet and triplet excided state absorption cross-sections respectively τ_{S_1}, and τ_{T_1} for the first singlet and triplet excited state lifetimes, τ_{ISC} for intersystem crossing time, and τ_{S_2} and τ_{T_2} for decay times from higher excited singlet and triplet states.

However, especially at higher input intensities, the model often needs to be modified further in order to be able to reproduce the recorded responses. A contribution of higher excited states or multiphoton absorptive processes, which in general necessitates higher inputs to evolve, might change the character of the NLA inducing switches from transmission drop to an increase or *vice versa*. Different models were proposed to explain switches in NLA behaviors. RSA switching to SA† was observed in the ps regime for texaphyrin derivatives,[6] 1,1',3,3,3',3'-hexamethylindotricarbocyanine iodide,[7] polymethine dyes[8] and azorene-appended phosphorus(V) tetratolylporphyrins,[9] to mention a few. In most cases, RSA/SA switch was attributed to the accumulation of population in higher excited singlet states which absorbed laser light weaker than the lower lying states and thus their contribution weakened the positive nonlinear absorption. Deng *et al*. also provided similar explanation of RSA/SA switch in their theoretical studies.[10] We recently reported a RSA/SA switch for 5,10-A_2B_2 porphyrins in the ns regime but could not fully explain the mechanism of the recorded behaviour.[11] It should be pointed out that such a behavior is uncommon for ns pulses. The opposite behavior, *i.e.* a SA response switching to RSA, has been observed both in the ns and ps regime for different materials (tetrabenzoporphyrin, [12]

subphthalocyanines,[13] linear polymers,[14] red dye[15] and ruthenium and osmium complexes of modified terpyridines[16]). In ns regime, RSA following SA was attributed to strongly absorptive one-photon processes arising from higher excited states. Singular reports attributed the switch in ns regime to TPA or to the absorption arising from metal to ligand charge transfer state. In ps regime the RSA following SA behavior was associated with TPA arising in the material or in the solvent. An interesting behavior - RSA/SA/RSA switch was observed for an 'axial-bonding' type hybrid porphyrin by Kiran *et al.* in the ps regime. This complex behavior was attributed to saturation of the excited state absorption followed by TPA.[18]

It can be concluded that switches in NLA response with input intensity involves complex photophysics. Likewise, simple models are often insufficient to explain responses which do not exhibit any switches, especially when higher input intensities are applied. *E.g.* Dini *et al.* proposed a model with TPA arising from the higher excited triplet state T_2 and another model with TPA arising from the S_1 state in order to explain transmission drop with intensity in hemiporphyrazine derivatives.[19]

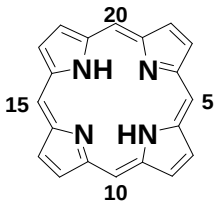

Figure 2: Numbering of meso positions in the porphyrin ring.

The distinct pattern, *i.e.* RSA/SA switch in the ns regime observed before for meso substituted 5,10-A_2B_2 porphyrins prompted us to investigate this class of compounds in more detail. Note, that related compounds with similar substituents though in a 5,15-A_2B_2 substitution pattern did not reveal any switch to SA at higher inputs (Fig. 2).[11]

Likewise, no RSA/SA switch was reported for broadly studied 5,10,15,20-tetrasubstituted compounds which can be found in literature.[1,20] This clearly demonstrates that 5,10-A_2B_2 compounds

exhibit distinct photophysical properties. Interestingly, our present studies on 5,10-A_2B_2 compounds provide further details on noteworthy NLA behaviors. The character of these responses was found to depend on structural features and the solvent used. Different models were considered in order to explain the observed phenomena and, as outlined below, the most successful model for all response types involved a four-level manifold where one-photon ESA was followed by instantaneous TPA arising from higher excited states. That suggests that despite varied structural features and conditions all 5,10-A_2B_2 compounds studied have similar excited state structures.

Experimental Methods

Materials: 5,10-A_2B_2 compounds were obtained starting from a 5,10-dibromo-15,20-di(*p*-tolyl)porphyrin (2H_Br) which synthesis was reported before.[21] Metalation of 2H_Br with $Zn(acac)_2$ or $Pd(acac)_2$ gave compounds Zn_Br and Pd_Br, respectively. Compounds 2H_Br and Zn_Br were then subjected to Sonogashira coupling with trimethylsilylacetylene (TMS-acetylene) which gave compounds 2H_CCTMS and Zn_CCTMS, respectively (Fig. 3). Instrumentation and standard techniques in material characterization used were as described before.[22]

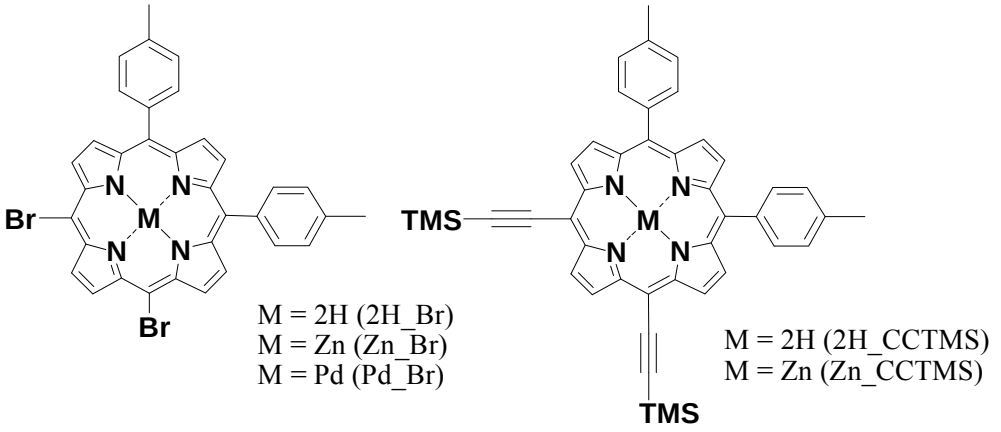

Figure 3: 5,10-A_2B_2 porphyrins.

General procedure for Sonogashira coupling: A Schlenk tube was filled with Ar and charged with brominated porphyrin (1 equiv.) in dry THF/NEt_3. The solution was degassed by three freeze-pump-

thaw cycles and put under Ar again. TMS-acetylene (4 - 5 equiv.), copper(I) iodine (0.25 equiv.) and $Pd(PPh_3)_2Cl_2$ (0.1 or 0.25 equiv.) were added, and the reaction mixture was stirred at room temperature until the starting material was consumed. Then CH_2Cl_2 (30 mL) was added and the solution was washed with water and dried over $MgSO_4$. Further purification was carried out as indicated.

(5,10-Dibromo-15,20-di(*p*-tolyl)porphyrinato)zinc(II) (Zn_Br): 5,10-Dibromo-15,20-di(*p*-tolyl)porphyrin 2H_Br (100 mg, 0.154 mmol) and $Zn(acac)_2$ (203 mg, 0.770 mmol) in 50 mL of toluene/MeOH (1:1, v:v) was brought to reflux. The progress of the reaction was monitored with TLC using $CHCl_3$/*n*-hexane (3:7, v:v) as eluent. The reaction was complete after 30 min. The solvent was removed and the product was isolated after passage through a plug of silica gel using $CHCl_3$ as eluent. Recrystallization of the residue from $CHCl_3$/MeOH yielded 108 mg (0.152 mmol) of the title product as shiny purple crystals (98%). M. p. > 300° ; R_f = 0.3 (SiO_2, $CHCl_3$/*n*-hexane 3:7, v/v); ^{1}H NMR (400 MHz, $CDCl_3$, 1% pyridine-d_5) δ = 2.68 (s, 6H, C*H*$_3$), 7.50 (d, 4H, *J* = 7.6 Hz, *H*$_{arom}$), 7.99 (d, 4H, *J* = 7.6 Hz, *H*$_{arom}$), 8.77 (s, 2H, β-*H*), 8.87 (d, 2H *J* = 4.7 Hz, β-*H*), 9.62 (d, 2H, *J* = 4.7 Hz, β-*H*), 9.73 (s, 2H, β-*H*) ppm; ^{13}C NMR (100.6 MHz, $CDCl_3$, 1% pyridine-d_5) δ = 21.5, 104.3, 122.2, 127.2, 132.3, 132.7, 133.3, 133.7, 134.4, 137.1, 139.9, 149.9, 151.0, 151.1 ppm; UV-vis (CH_2Cl_2): λ_{max} (log ε) = 393 (4.83), 424 (5.59), 517 (3.73), 554 (4.33), 595 nm (3.69); HRMS (MALDI LD+) calcd. for $C_{34}H_{22}N_4Br_2Zn$ $[M]^+$ 707.9503, found 707.9478, HRMS (ES+) $C_{34}H_{22}N_4Br_2Zn$ $[M]^+$ calcd. 707.9503, found 707.9529.

(5,10-Dibromo-15,20-di(*p*-tolyl)porphyrinato)palladium(II) (Pd_Br): 5,10-Dibromo-15,20-di(*p*-tolyl)porphyrin 2H_Br (100 mg, 0.154 mmol) and $Pd(acac)_2$ (52 mg, 0.171 mmol) were dissolved in toluene (15 mL) and heated under reflux for 5 h. The progress of the reaction was monitored by TLC using CH_2Cl_2/*n*-hexane (4:1). Upon completion of the metalation the solvent was removed *in vacuo* and the product isolated after passage through a plug of silica gel using $CHCl_3$ as eluent. Product recrystallization using CH_2Cl_2/MeOH yielded 83 mg of red crystals (0.110 mmol, 63 %). M. p. > 300°

C; R_f = 0.42 (SiO_2, CH_2Cl_2/*n*-hexane 4:1, v/v); ^{1}H NMR (400 MHz, $CDCl_3$) δ = 2.73 (s, 6H, C*H*$_3$), 7.57 (d, 4H, *J* = 7.8 Hz, H_{arom}), 8.01 (d, 4H, *J* = 7.8 Hz, H_{arom}) 8.76 (s, 2H, β-*H*), 8.85 (d, 2H *J* = 4.9 Hz, β-*H*), 9.57 (d, 2H, *J* = 4.9 Hz, β-*H*), 9.62 (s, 2H, β-*H*) ppm; ^{13}C NMR (100.6 MHz, $CDCl_3$) δ = 21.5, 105.2, 123.0, 127.6, 131.7, 132.2, 132.5, 132.8, 133.9, 137.8, 138.2, 141.5, 141.6, 142.3, 142.6 ppm; UV-vis (CH_2Cl_2): λ_{max} (log ε) = 422 (3.66), 531 (2.73), 656 nm (2.18); HRMS (MALDI LD+): calcd. for $C_{34}H_{22}N_4Br_2Pd$ $[M]^+$ 749.9246, found 749.9268.

5,10-Di(*p*-tolyl)-15,20-bis[(trimethylsilyl)ethynyl]porphyrin (2H_CCTMS)**:** Following the general procedure for Sonogashira coupling, 90 mg (0.139 mmol) of porphyrin 2H_Br, 0.096 ml (0.692 mmol) of TMS-acetylene, 6 mg (0.032 mmol) of CuI and 9 mg (0.013 mmol) of $Pd(PPh_3)_2Cl_2$ in 40 mL of THF/NEt_3 (1:3, v/v) after 12 h gave 64 mg (0.093 mmol, 67%) of a dark green solid after purification by column chromatography on silica gel (CH_2Cl_2/*n*-hexane 1:3 v/v). M. p. = 294 °C; R_f = 0.43 (SiO_2, CH_2Cl_2/*n*-hexane 1:3, v/v); ^{1}H NMR (400 MHz, $CDCl_3$) δ = -2.11 (br, 2H, N*H*), 0.65 (s, 18H, C*H*$_3$), 2.73 (s, 6H, C*H*$_3$), 7.58 (d, 4H, *J* = 7.8 Hz, H_{arom}), 8.06 (d, 4H, *J* = 7.8 Hz, H_{arom}), 8.73 (s, 2H, β-*H*), 8.86 (d, 2H, *J* = 4.9 Hz, β-*H*), 9.57 (d, 2H, *J* = 4.9 Hz, β-*H*), 9.69 (s, 2H, β-*H*) ppm; ^{13}C NMR (150.90 MHz, $CDCl_3$) δ = 0.2, 21.4, 99.6, 102.0, 106.5, 122.8, 127.4, 134.2, 137.5, 138.5 ppm; UV-vis (CH_2Cl_2): λ_{max} (log ε) = 439 (2.92), 541 (1.7), 581 (1.89), 618 (1.61), 679 nm (1.64); HRMS (ES+) $C_{44}H_{43}N_4Si_2$ $[M+H]^+$ calcd. 683.3026, found 683.3031.

{5,10-Di(*p*-tolyl)-15,20-bis[(trimethylsilyl)ethynyl]porphyrinato}zinc(II) (Zn_CCTMS)**:** Following the general procedure for Sonogashira coupling, 240 mg (0.377 mmol) of porphyrin Zn_Br, 0.233 ml (1.679 mmol) of TMS-acetylene, 16 mg (0.084 mmol) of CuI and 24 mg (0.034 mmol) of $Pd(PPh_3)_2Cl_2$ in 45 mL of THF/NEt_3 (1:2, v/v) after 12 h gave 235 mg (0.315 mmol, 84 %) of a violet solid after isolation of the product after passage through a plug of alox using $CHCl_3$ as eluent. M. p. > 300 °C; R_f = 0.4 (SiO_2, EtOAc/*n*-hexane 1:9, v/v); ^{1}H NMR (400 MHz, $CDCl_3$, 1% pyridine-d_5) δ = 0.56 (s, 18H, C*H*$_3$), 2.63 (s, 6H, C*H*$_3$), 7.46 (d, 4H, *J* = 7.6 Hz, H_{arom}), 7.96 (d, 4H, *J* = 7.6 Hz, H_{arom}),

8.69 (s, 2H, β-*H*), 8.82 (d, 2H *J* = 4.1 Hz, β-*H*), 9.56 (d, 2H *J* = 4.1 Hz, β-*H*), 9.67 (s, 2H, β- *H*) ppm; ^{13}C NMR (150.90 MHz, $CDCl_3$, 1% pyridine-d_5) δ = 0.4, 21.4, 99.3, 100.2, 108.4, 123.7, 127.1, 130.3, 131.5, 131.6, 132.8, 134.3, 136.9, 139.8, 149.6, 150.2, 152.5, 152.7 ppm; UV-vis (CH_2Cl_2): λ_{max} (log ε) = 441 (5.7), 5.72 (4.5), 615 nm (4.5); HRMS (ES+) $C_{44}H_{41}N_4ZnSi_2$ $[M+H]^+$ calcd. 745.2161, found 745.2197.

Nonlinear absorption: The open Z-scan technique[23] was used to measure NLA of 5,10-A_2B_2 porphyrins. Briefly, the open Z-scan technique measures total transmittance through the sample as the function of incident laser intensity while the sample is gradually moved along focused Gaussian beam. A 6 ns Q-switched Nd:YAG laser operating at second harmonic of 532 nm with a pulse repetition rate of 10 Hz was used in all open Z-scan experiments. The beam was spatially filtered to remove higher order modes and tightly focused with a 9 cm focal length lens. Samples were prepared by dissolving porphyrin in spectroscopic grade toluene and DMF at a concentration of 2.5×10^{-4} M followed by gentle agitation for about 1 hour in a low power sonic bath. Additionally for compound Pd_Br, studies were carried on more dilute samples at a concentration of 2.5×10^{-5} M. Samples were freshly prepared prior to experiments. All measurements were performed in a quartz cell with 1 mm path length. For each sample several scans were run. For each following scan the energy was increased by approximately 20 μJ starting from 35 μJ until symmetric reproducible data were obtained. Ground state absorption spectra were recorded with a Shimadzu multiSpec-1505 instrument.

Results

The ground state absorption spectra of porphyrins exhibit two characteristic features – a high energy Soret and low energy Q bands (Fig. 4). The Soret band maxima of the two compounds 2H_CCTMS and Zn_CCTMS with TMS-ethynyl groups are red-shifted in reference to brominated compounds

Zn_Br and Pd_Br, which is expected for compounds with an extended conjugated system. The Q-bands were observed in similar wavelength ranges for all compounds and the experimental wavelength of 532 nm is situated in their close proximity. An exception is compound Pd_Br, for which the Q-band maximum is equal to 532 nm. The number of Q-bands of the metalated porphyrins Zn_Br, Pd_Br and Zn_CCTMS is reduced to two in reference to free-base compound 2H_CCTMS with four Q-bands. Reduction in the number of Q-bands is commonly observed upon metalation due to an increase in the symmetry of the porphyrin core.[24]

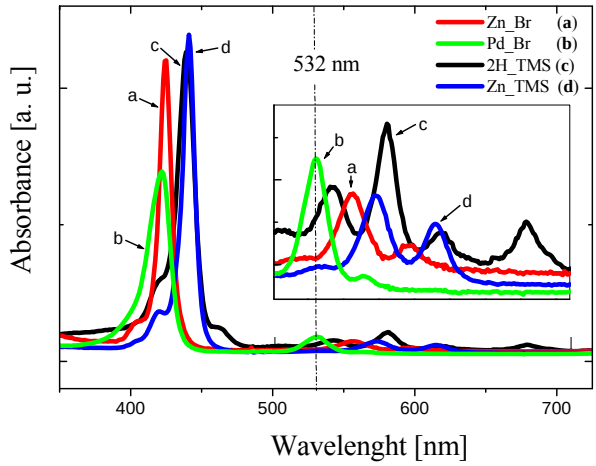

Figure 4: Ground state absorption spectra of Zn_Br, Pd_Br, 2H_CCTMS and Zn_CCTMS in CH_2Cl_2. Inset shows the Q-band area.

We first carried out open Z-scan studies on Zn_Br, Pd_Br, 2H_CCTMS and Zn_CCTMS in toluene (Fig. 5 upper row). An interesting NLA was observed for 2H_CCTMS, for which at higher input laser energy experiments two distinctive parts became apparent in the Z-scan trace. Steep drop in transmission could be seen in close focal area, whereas further apart from the focus transmission drop was gentler. We will refer to this type of behavior as RSA/RSA switch. Zn_Br provided a response profile similar to 2H_CCTMS, however, with much smoother transition between the two parts. The character of the Z-scan response recorded for Zn_CCTMS was much broader in reference to the previous compounds, with no distinctive parts in Z-scan trace. Pd_Br with high linear absorption at the

experimental wavelength exhibited an increase in transmission followed by a decrease closer to the focal regime, which switched again to an increase even closer to the focal regime. We refer to this response as SA/RSA/SA switch. However, symmetric reproducible responses for this compound could only be obtained at very low input energies. Once the input energy was increased the Z-scan response became asymmetric, indicating a degenerative process. High linear absorption, as exhibited by this compound, should enhance such processes. Clearly, none of the responses observed in toluene exhibited the characteristic RSA/SA switch which was observed before for 5,10-A_2B_2 compounds in DMF. As the solvent is known to affect the NLA properties of RSA materials we carried out further studies in DMF.[25, 26] DMF was a poor solvent for compounds Pd_Br and 2H_CCTMS in comparison with toluene, whereas for compounds Zn_Br and Zn_CCTMS it provided good solubility. It is known that DMF coordinates to zinc ions. Since both compounds Zn_Br and Zn_CCTMS bears zinc in the central core, their good solubility in DMF can be associated with the coordination of the solvent molecules to the metal in the central core. It turned out that much higher input energies can be applied in Z-scan experiments in DMF than in toluene. Good quality, symmetric and reproducible data were obtained in DMF at high input energies. In contrast, at similar inputs some asymmetric features in the Z-scan trace especially in the focal regime were observed in toluene, implying a degenerative process. The evolutions of the responses recorded in DMF for all porphyrins studied are presented in Fig.5 (lower row).

Clearly, the solvent affected the character of the response. The RSA/RSA character of 2H_CCTMS in toluene changed to RSA/weak SA/RSA/SA. For Zn_Br and Zn_CCTMS a switching from RSA to SA in the focal regime in the experiments carried out at higher input energies was observed. A SA/RSA/SA type response was detected for Pd_Br in DMF, as it was in toluene. However, the SA/RSA/SA Z-scan trace profile became apparent only in experiments at higher input energies in DMF, which were inaccessible for toluene. At lower inputs only SA was detected in DMF which

evolved to SA/RSA when the input was increased and finally to SA/RSA/SA at even higher inputs.

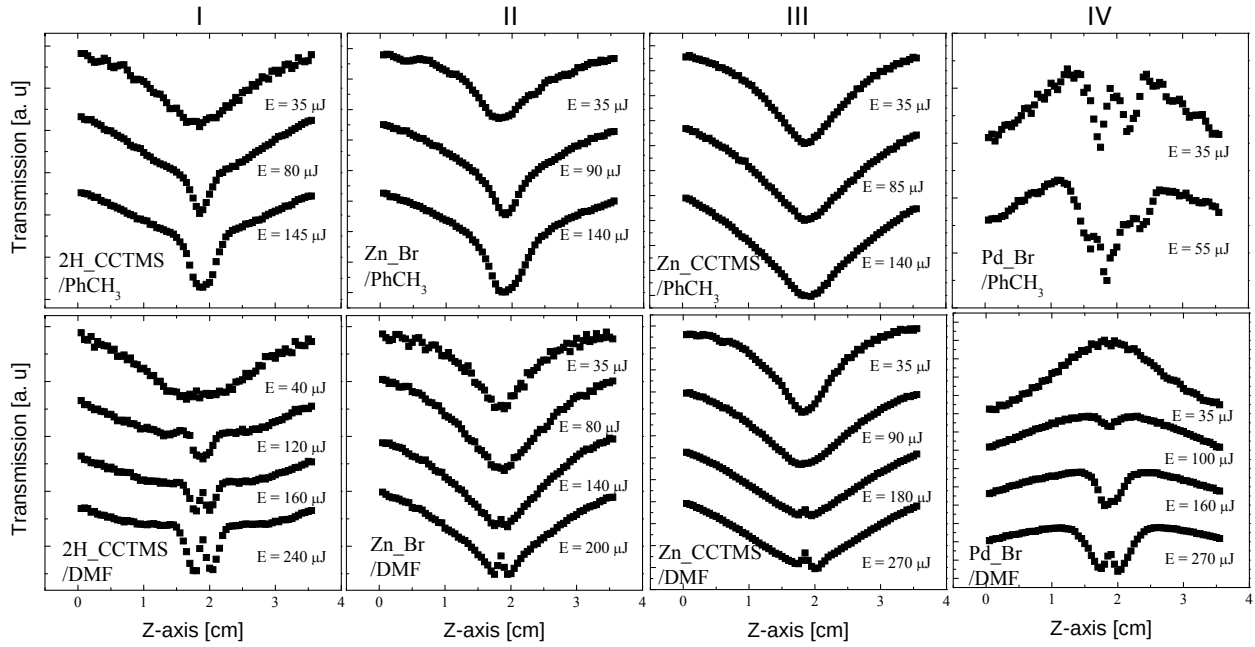

Figure 5: Each box illustrates the evolution of the Z-scan response for the following experiments carried out at increasing input energy for a given compound. Each column show results for one compound: column I - 2H_CCTMS, column II - Zn_Br, column III - Zn_CCTMS and column IV - Pd_Br. Upper row shows experiments carried out in toluene, lower row - in DMF.

Modelling studies: RSA arises in porphyrins in the spectral window between the Soret and Q-bands. The transmission drop with intensity observed for Zn_Br, 2H_CCTMS and Zn_CCTMS was attributed to such a process. It should dominate at lower fluences before higher excited states become populated. The SA character of the response observed for Pd_Br indicated that the cross-section of the excited state was smaller than that of the ground state. In order to explain subsequent switches following RSA or SA behavior, additional processes have to be considered.

The following assumptions were made in modeling the NLA responses. We assumed that the triplet state T_1 is quickly and efficiently populated through ISC. Typically τ_{ISC} is on the order of nanosecond

or shorter for porphyrins and is shorter for compounds with heavy atoms in the central core or the molecular periphery (such as halogen atoms). Introduction of heavy metal atoms not only improves the ISC rate but also enhances the yield for triplet state formation φ_T.[27,28] *E.g.* φ_T = 1 and φ_T = 0.83 were reported for lead and zinc complexes of 5,10,15,20-tetra[(trimethylsilyl)ethynyl]porphyrin respectively. Similar φ_T were obtained for the same metal complexes of 5,10,15,20-tetraphenylporphyrin (*i.e.* φ_T = 1 for lead complex and φ_T = 0.82 for zinc complex). The fluorescence lifetime and ISC time were both ~ 2 ns, for the zinc complexes.[27] As far as halogenated porphyrins are concerned, φ_T being in the range of 0.8 – 1 and fluorescence lifetimes and ISC times being below 1 ns, were reported before.[28] Therefore, the assumption that the triplet state T_1 is quickly and efficiently populated through ISC should be valid, especially for metalated and brominated compounds, under ns pulsed laser used in the studies. Based on that assumption the contribution of the absorption arising from S_1 state to the measured response can be neglected under ns pulses. Instantaneous TPA arising from the ground state can be ignored at the experimental wavelength and under ns pulse duration. Concerning the latter statement, different approaches were described by various groups in the literature, which either consider or neglect the contribution of instantaneous two-photon absorption arising from the ground state at close to resonant wavelength range in the ns regime.[12, 29, 27] We applied a steady-state approximation which assumes that the population of electronic states does not vary within the pulse width ($dN_i/dt = 0$). The steady-state approximation is valid when the pulse width is much longer than relaxation times. Different authors demonstrated that such an assumption approximated well dynamic models. Gao *et al.* proved that such an approximation is valid while modelling the SA/RSA type of behavior of a linear polymer in the ns regime with a four-level mode.[14] O'Flaherty *et al.* showed that a steady-state model approximated well the NLA response of phthalocyanines in the ns regime.[30] They also demonstrated that the five-level Jablonski model can be simplified with a three-level model provided that ISC is fast and efficient. According to the three-level

model, NLA is entirely due to T_1-T_2 ESA transitions. Effectively, such a model is equivalent to model A presented in Fig. 6, where the lifetime of state N_1 is actually the lifetime of state S_1 and the absorption arising from the state N_1 is attributed to T_1-T_2 transitions. We considered different models by addition of subsequent higher excited states (Fig. 6). The populations of the highest excited state were neglected for each of these models.

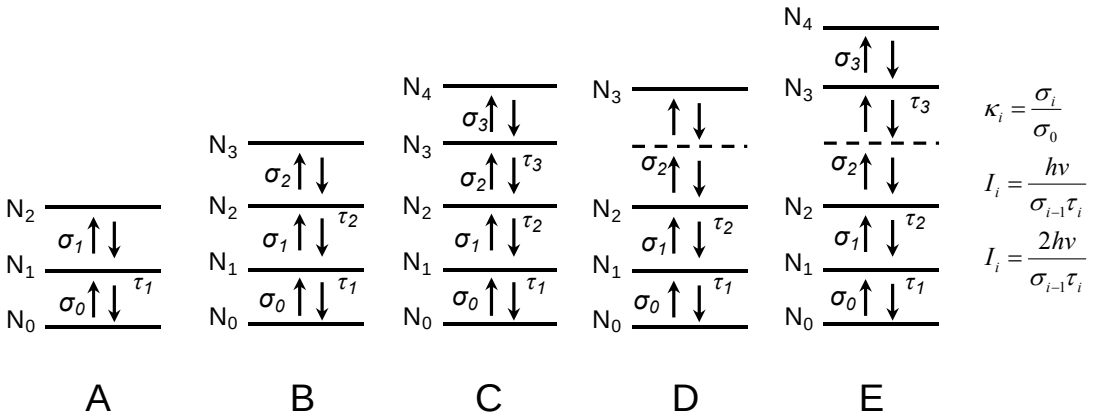

Figure 6: Schematic illustration of different models **A**-**E** considered in modeling studies along with the definition of fitting parameters κ_i and I_i. σ_i stands for the cross-sections of the ground (i=0) and excited states ($i \geq 1$), τ_i for the lifetime of i-th state. κ_i is the ratio of the excited state absorption cross-section σ_i to that of the ground state σ_0. I_i is saturation intensities of one- or two-photon absorption processes.

Rate equations and the expression for the nonlinear absorption coefficient as a function of input intensity $\alpha(I)$ obtained from analytical solutions of these equations are presented in the Appendix for all models. The expressions $\alpha(I)$ (Eq. A11, Eq. A18, Eq. A25, Eq. A27, Eq. A32) were implemented to the propagation equation (Eq. 1):

$$\frac{dI}{dz'} = -\alpha(I)I \qquad \text{(Eq. 1)}$$

and was used to fit the recorded responses. Propagation equations for a given model were implemented into computational code. For each position along the Z-axis the expressions were

integrated over z' from 0 to L, where L is the sample thickness, and divided by input intensity recalculated according to:

$$I_0 = \frac{2E}{\pi^{3/2}\tau\omega_0{}^2[1+(z/z_0)^2]}^{31} \qquad \text{(Eq. 2)}$$

where E stands for pulse energy, τ for pulse width, ω_0 for beam radius at the focus (ω_0 = 18-24 μm), z for the sample position along the Z-axis and z_0 for diffraction length of the beam which equals to:

$$z_0 = \pi\omega_0{}^2/\lambda \qquad \text{(Eq. 3)}$$

λ is a laser wavelength. In order to obtain approximate normalized transmission values, in first instance the integrated expressions were divided by a far field linear transmission, which was measured. It can be seen that no pure linear regime could be reached for the compounds studied even for the lowest possible input energy experiments. Yet, except for Pd_Br, the lowest input energy curves are "close" to being flat in the far field. Therefore, it is assumed that lowest input energy experimental curves are close to the linear regime in the far field. During the fitting the experimental curves were allowed to vary its position along y-axis (normalized transmission) within a few percents from normalized transmission being equal to unity (in the far field) to provide the best fit possible. It is believe that, besides Pd_Br which exhibited distinct character of the curve, the procedure applied should not affect significantly fitting parameters.

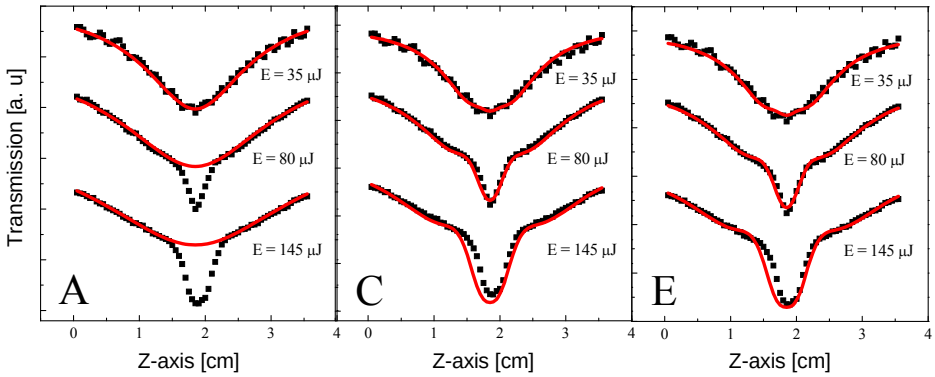

Figure 7: Comparison of the fitting curves (red lines) obtained with models **A**, **C** and **E** for the experiments carried out at increasing input energy for compound 2H_CCTMS in toluene. The following set of parameters were used in the fittings: model **A**: I_1 = 0.14 GW cm^{-2}, σ_1 = 1.65; model **C**: I_1 = 0.13 GW cm^{-2}, I_2 = 0.4 GW cm^{-2}, I_3 = 1.7 GW cm^{-2}, σ_1 = 2.3, σ_2 = 0, σ_3 = 6.3; model **E**: I_1 = 0.45 GW cm^{-2}, I_2 = 0.1 GW cm^{-2}, I_3 = 2.05 GW^2 cm^{-4}, σ_1 = 4.4, σ_2 = 2.8 cm^2 GW^{-1}, σ_3 = 0. ■ represents experimental data.

We first focused our attention on the NLA response of 2H_CCTMS. As illustrated in Fig. 7, model **A** provided good fitting only for the experiments recorded at low input energies. For experiments at higher input energies, where RSA/RSA switching became apparent, the fitting curve followed well only the part of the curve further from the focus. This suggests that the response arising at lower fluences would proceed through a sequential absorption of two photons. Model **B**, created by adding one more higher excited state, could not reproduce the steep drop in transmission appearing in the focal area in higher input energy experiments. Moreover, fitting of the "less steep" part of the curve was less precise in comparison to the previous model (data not shown). This reinforced the assumption that absorption in the lower fluence regime arises through sequential absorption of two photons. Interestingly, fitting based on the five-level model **C** was far more improved and could reproduce the characteristic RSA/RSA shape.

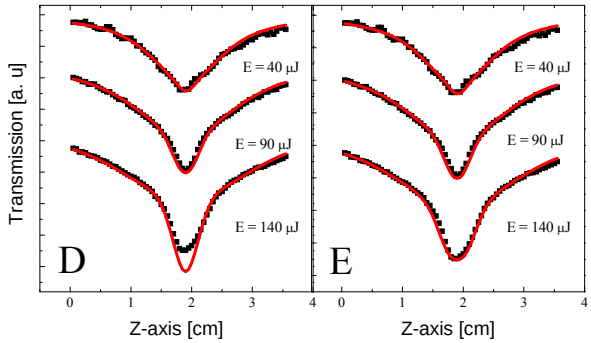

Figure 8: Comparison of the fitting curves (red lines) obtained with models **D** and **E** for the experiments carried out at increasing input energy for compound Zn_Br in toluene. The following set of parameters were used in the fittings: model **D**: I_1 = 0.29 GW cm^{-2}, I_2 = 0.2 GW cm^{-2}, β_1 = 5.3, β_2 = 4.2 cm^2 GW^{-1}; model **E**: I_1 = 0.3 GW cm^{-2}, I_2 = 0.16 GW cm^{-2}, I_3 = 2.2 GW^2 cm^{-4}, β_1 = 5.4, β_2 = 5.6 cm^2 GW^{-1}, β_3 = 0. ■ represents experimental data.

Meanwhile, it was observed that the RSA/RSA switch is reproduced best when $\kappa_2 = 0$. Only for experiments at higher input energies did the response predicted by the model slightly diverge from the experimental data, *i.e.* reaching slightly lower transmission values than those actually recorded. $\kappa_2 = 0$ means that absorption arising from state N_2 is insignificant. This is the absorption arising from state N_3 which grants good fitting of the "steep" part of the curve in the close focal regime. The absorption arising from state N_2 and N_3 are associated with terms in the numerator of the expression for the nonlinear absorption coefficient (Eq. A25), depending respectively upon second and third power of intensity. Since the second power term is insignificant and the third power term grants good fitting of the response in the close focal regime, yet another model **D** with the expression for the nonlinear coefficient with no second but only third order term was proposed (Eq. A27). The population of the state N_2 is transferred into higher level state in one step TPA in model **D** instead of two sequential one-photon absorption processes as in model **C**. A similar model with TPA arising from the T_2 excited

state was previously proposed for a hemiporphyrazine derivative.[19] Such a four-level model **D** provided a similar fitting quality to that observed for model **C** with a slight divergence from the experimental data at higher input energies. This could suggest the saturation of higher excited states. The fitting at higher inputs was improved when the population of state N_3 was taken into account in the total population (model **E**). At the same time absorption arising from N_3 state was set to 0 i.e. $\kappa_3 = 0$. In reference to theoretical studies on NLA switches cited before, it can be predicted that at even higher fluences, if those were accessible, switching to SA should be observed, since $\kappa_3 = 0 < 1$ and $\kappa_2 > 1$.[9]

Similar observations were made in reference to modelling the response for compound Zn_Br. A five-level model with subsequent one-photon absorptive processes **C** could reproduce the response as well as a four-level model with two-photon absorption process arising from the excited state **D**. The term with parameter κ_2 in the expression for the NLA coefficient Eq. 25 describing model **C** had much less effect on the fit quality than the remaining terms and could be neglected. Analogously to previous studies, both models **C** and **D** predicted a larger transmission drop than actually observed in experiments carried out at higher input energies. This deviation was more pronounced for compound Zn_Br compared to 2H_CCTMS. The fitting was improved when the population of state N_3 (model **E**) was taken into account (Fig. 8). Clearly, the population of state N_3 cannot be neglected. Likewise absorption arising from that state is negligible. Best fit was obtained when $\kappa_3 = 0$.

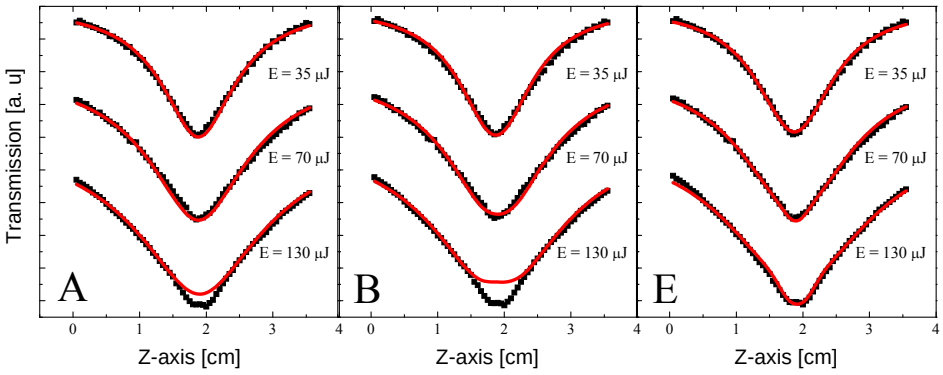

Figure 9: Comparison of the fitting curves (red lines) obtained with models **A**, **B** and **E** for the experiments carried out at increasing input energy for compound Zn_CCTMS in toluene. The following set of parameters were used in the fittings: model **A**: I_1 = 0.12 GW cm^{-2}, σ_1 = 4.2; model **B**: I_1 = 0.14 GW cm^{-2}, I_1 = 0.9 GW cm^{-2}, σ_1 = 4.3, σ_2 = 3.2; model **E**: I_1 = 0.17 GW cm^{-2}, I_2 = 0.5 GW cm^{-2}, I_3 = 1.7 GW^2 cm^{-4}, σ_1 = 5.2, σ_2 = 6.5 cm^2 GW^{-1}, σ_3 = 0. ■ represents experimental data.

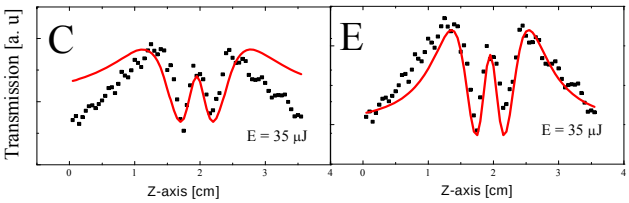

Figure 10: Comparison of the fitting curves (red lines) obtained with models **C** and **E** for compound Pd_Br in toluene. The following set of parameters were used in the fittings: model **C**: I_1 = 0.1 GW cm^{-2}, I_2 = 0.08 GW cm^{-2}, I_3 = 0.4 GW cm^{-2}, σ_1 = 0.05, σ_2 = 2, σ_3 = 0; model **E**: I_1 = 0.08 GW cm^{-2}, I_2 = 0.07 GW cm^{-2}, I_3 = 0.036 GW^2 cm^{-4}, σ_1 = 0.75, σ_2 = 11.5 cm^2 GW^{-1}, σ_3 = 0. ■ represents experimental data.

Next we analyzed the response of compound Zn_CCTMS which exhibited a much broader Z-scan trace (Fig. 9). Both three- and four-level models with sequential absorption of two and three photons **A** and **B**, respectively, provided comparable good quality fits for the low and moderate input energy data but no longer followed the response at higher input energies. Evidently, model **E** with TPA arising from the excited state provided the best fit for the results at both low and high inputs. Absorptive processes arising from the state N_3 (*i.e.* $\kappa_3 = 0$) were neglected as before.

Compound Pd_Br exhibited an interesting response, *i.e.* a SA/RSA/SA switch. As stated before no good quality data could be obtained at moderate and higher input energies for the compound. As soon as the input energy was increased the Z-scan response became asymmetric. The two switches in the Z-scan trace suggested that at least the five-level model is needed to reproduce the response, provided

that consecutive absorptive processes are considered. Models **C** and **E** were investigated in modeling the response of compound Pd_Br in toluene. Model **E** provided a better fit to the experimental data (Fig. 10).

Similar modeling studies were carried out for the responses recorded in DMF for all compounds. Again, model **E** provided the best fitting among all of models considered. However, once a final switch to SA in the higher fluence regime was observed, the predicted response started to deviate more and more from the recorded data for subsequent experiments carried out at increasing input energy. The response predicted by the model could not reach the minimal transmission recorded for the compound. It also could not reproduce the SA peak observed experimentally in the close focal regime. (An example: compound 2H_CCTMS in Fig. 11a, red line represents fitting with model **E**). Similar observations were made for all other compounds in DMF. We concentrated on the analysis of the response of compound 2H_CCTMS. It was found that the fitting quality improved when parameter κ_3 was allowed to take variable (increasing) values for the subsequent experiments at higher inputs (Fig. 11a, blue line represents curves based on model **E** with varied values of parameter κ_3). This indicates that further absorptive processes arising from state N_3 cannot be neglected at very high input energies. Note that none of the fitting parameters varied between subsequent experiments at increasing input energy. However, as the unusual behavior of parameter κ_3 was observed for high input energy experiments, possibly the parameter is affected by thermal effects. These effects can originate fromthe conformational changes that affect excited states and transitions. We re-treated data obtained for compound 2H_CCTMS in DMF at higher input energies and plotted them as normalized transmission *versus* pulse energy density (Fig. 11b). It can be seen from the figure that the experimental data for the subsequent experiments does not recover in higher fluence range. RSA/SA turnover fluence increases and that the minimal transmission reaches lower values, for each of the following experiment carried at increasing input energy. The same was observed for the other compounds in DMF. Such a behavior

indicates that some additional processes contribute to the NLA signal at higher fluences. We associate this processes with thermally affected absorption arising from the state N_3.

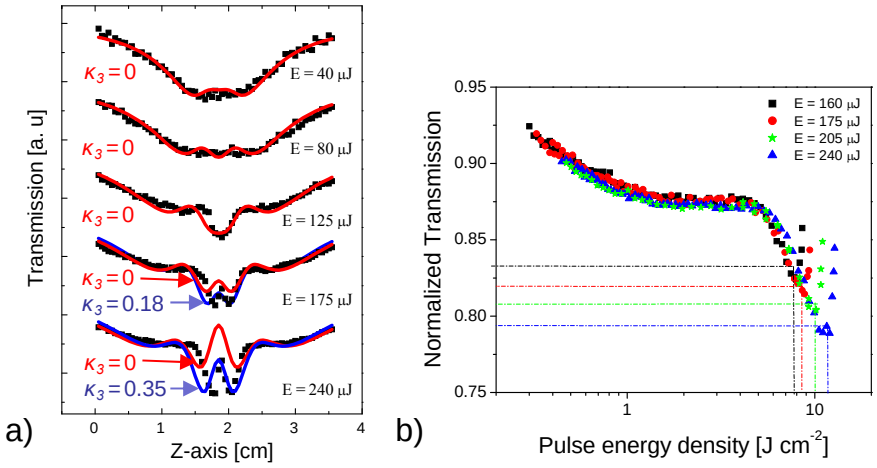

Figure 11: a) Experimental data (■) for compound 2H_CCTMS in DMF at increasing input energy along with fitting curves. Red lines represent fitting curves obtained with model **E** while keeping all parameters constant for all of the experiments (I_1 = 0.48 GW cm^{-2}, I_2 = 0.14 GW cm^{-2}, I_3 = 2 GW^2 cm^{-4}, β_1 = 3.7, β_2 = 2 cm^2 GW^{-1}, β_3 = 0); blue lines represent fitting curves based on the same model with varied values of parameter β_3 for the experiments at high inputs while keeping the values of all of the rest parameters constant and equal to those in previous case. b) High input energy data plotted as normalized transmission versus pulse energy density.

Table 1 Best fit parameters (model **E**) for 5,10-A_2B_2 porphyrins in toluene (T) and DMF (D).

Parameter $\kappa_3 = 0$ in all cases.

Por/ Solvent	α_0 $[cm^{-1}]$	κ_1	κ_2 $[cm^2GW^{-1}]$	I_1 $[GWcm^{-2}]$	I_2 $[GWcm^{-2}]$	I_3 $[GW^2cm^{-4}]$
Zn_Br/T	1.73	5.4	5.5	0.3	0.16	2.2
Zn_Br/D	1.38	4.7	3.7	0.38	0.3	1.65
2H_CCTMS/T	3.96	4.4	2.8	0.45	0.1	2.05
2H_CCTMS/D	3.54	3.7	2	0.48	0.14	2
Zn_CCTMS/T	2.3	5.2	6.5	0.17	0.5	1.7
Zn_CCTMS/D	1.84	5	6.4	0.14	2	1.5
Pd_Br/T	6.32	0.75	11.5	0.08	0.07	0.036
Pd_Br/D	6.72	0.4	1.1	0.013	3	1.8

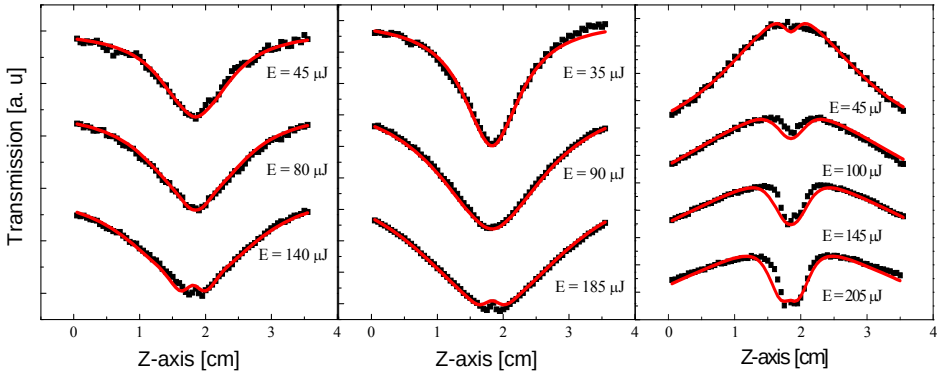

Figure 12: Illustration of the experimental data (■) obtained at increasing input energy for compounds Zn_Br, Zn_CCTMS and Pd_Br in DMF (left to right) along with fitting curves (red lines) based on model **E**. Fitting parameters used in the modelling are summarized in Table 1.

Fig. 12 shows the fitting curves obtained with model **E** for the other compounds (Zn_Br, Zn_CCTMS and Pd_Br) in DMF. Only the experimental data, for which the model provided good fit

with $\kappa_3 = 0$, are presented.

Discussion

The diverse range of profiles of the Z-scan traces recorded for 5,10-A_2B_2 porphyrins could suggest different NLA processes for different compounds. However, it was shown that the five-level model **E** provided the best fit for all compounds, implying that all compounds exhibit similar excited state behavior. Best fit parameters used in modeling the recorded responses are compiled in Table 1. With the parameter $\kappa_3 = 0$ used in all fittings, the model can actually be reduced to a four-level manifold where population of the highest excited state N_3 is not neglected. The applicability of such a model to the NLA responses of 5,10-A_2B_2 compounds reveals that their excited state structure differs from that of other meso tetrasubstituted porphyrins[20] and resembles that of a hemiporphyrazine derivative.[19] For the latter the model with instantaneous TPA from higher excited state applied to only one compound (chloroindium hemiporphyrazine derivative), whereas it was not applicable to the related lead complex or similar compounds. As a result and in reference to the present study, it is difficult to delineate common structural features that lead to distinct NLA mechanism.

The model was developed based on the steady state approximation. Additionally, it was assumed that ISC is fast and efficient. Such assumptions should be valid for metalated compounds however, further studies are needed to elucidate the photophysical properties of the 5,10-A_2B_2 compounds in more detail. This would enable a validation of the mechanism. The ISC rate and the quantum yield for triplet state formation are usually lower for free base porphyrins.[27, 32] Thus, the assumptions applied in the present model might not necessarily be valid for free base compound 2H_CCTMS. However, for the sake of simplicity, here the same model was used for the free base compound and the model did reproduce the recorded response of compound 2H_CCTMS well. Thus, we believe that the parameters can be used for comparative studies, bearing in mind, the assumptions applied.

The character of the Z-scan traces recorded in toluene and DMF for compound Zn_CCTMS were

broader compared to those for compounds Zn_Br and 2H_CCTMS. A broadening of Z-scan wings was observed by Kimball *et al.* when investigating solvent effects on the NLA of (tetrabenzoporphyrinato)zinc(II).[25] The broadening was attributed to a contribution of triplet excited state cross-section and larger ISC rate. In our case we associate the broadening with an increase in κ_1 and κ_2 combined with a decrease in I_1. κ_1 and κ_2 increase and I_1 decrease for the compounds in the following order: Zn_Br, 2H_CCTMS and Zn_CCTMS. Lower I_1 provides that saturated regime of NLA is reached at lower inputs, which enhances effective contribution of ESA to the NLA response. Likewise, ESA is enhanced by large ISC rate.

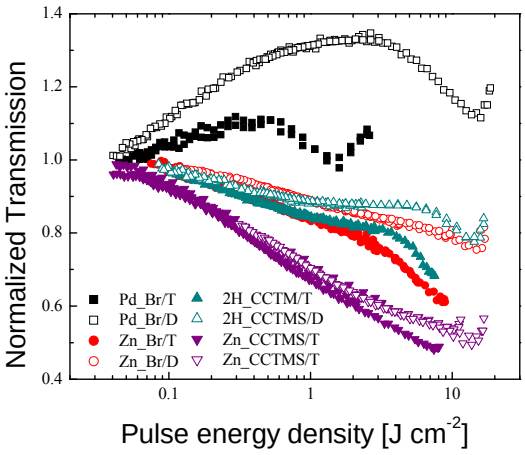

Figure 13: Experimental data shown as normalized transmission versus pulse energy density for all compounds in toluene (T) and DMF (D).

Compound 2H_CCTMS showed a RSA/RSA response in toluene and RSA/weak SA/RSA/SA in DMF. A RSA/SA/RSA profile was reported before in the ps regime for porphyrin arrays and was attributed to saturation of ESA followed by TPA.[18] The profile of the Z-scan response of compound 2H_CCTMS in DMF is explained with similar processes. We attribute RSA/SA observed at lower intensities with saturation of one-photon excited state absorption. The following switch in the closer

focal regime arises due to TPA from the higher excited triplet states (rather than from S_0 as in porphyrin arrays). The final switch to SA is associated with saturation of the two-photon absorption. The different NLA responses in the two solvents studied are associated with κ_1 and κ_2 being higher in toluene than in DMF as I_1, I_2 and I_3 did not vary significantly between the solvents.

The experimental data obtained for all compounds in toluene and DMF were manipulated and plotted as normalized transmission *versus* pulse energy density (Fig. 13). The parameters κ_1 and κ_2, being the ratios of the higher excited states cross-sections to that of the ground state, were larger in toluene than in DMF for all compounds. This indicates the solvent impact on the NLA parameters, which is in agreement with earlier reports.[25,33] For all compounds with an overall transmission drop with intensity (Zn_Br, 2H_CCTMS and Zn_CCTMS) the transmission reached a lower minimal value in toluene than in DMF. This was associated with higher values of parameters κ_1 and κ_2 in toluene. Additionally, the linear absorption at the experimental wavelength 532 nm was higher in toluene than in DMF for compounds Zn_Br, 2H_CCTMS and Zn_CCTMS. A higher ground state absorption would result in larger population of the excited state which should contribute to the larger transmission drop observed in toluene. Note, that all compounds in DMF exhibited switching to SA at higher fluences. At such high fluences asymmetric and nonreproducible Z-scan data were recorded in toluene. Except for compound Pd_Br, none of the compounds exhibited switches to SA in toluene in the fluence regime investigated. However, as discussed before, a RSA/SA switch would be expected to occur for those compounds if a higher fluence range was experimentally accessible in toluene. This behavior can be expected for $\kappa_2 > 1$ and $\kappa_3 = 0 < 1$, in reference to theoretical studies reported before.[9]

Zn_CCTMS exhibited the largest transmission drop in both solvents in reference to the analogous free base compound 2H_CCTMS and the brominated zinc complex Zn_Br. This makes Zn_CCTMS most promising for application as an optical limiting (OL) material against green laser light. The result agrees well with general trends observed for macrocyclic dyes, according to which, firstly, compounds

with extended conjugation provide better OL efficiency and, secondly, metal complexes outperform free base compounds.[20] In addition, meso tetrasubstituted porphyrins with TMS-ethynyl groups were reported to be highly potential OL candidates.[27] In agreement we showed in previous studies, that a 5,15-A_2B_2 porphyrin with TMS-ethynyl groups provided much better OL performance than porphyrins with other substituents.[34] Thus, the present study reinforces the utility of the TMS-ethynyl group as a very useful substituent for OL porphyrins. Compound Zn_Br reached slightly lower minimal transmission than compound 2H_CCTMS in both solvents. Evidently, a combination of structural features such as heavy atoms (here bromine atoms at the meso position and the central metal compound Zn_Br) did not yield a material superior to the free base compound 2H_CCTMS with an extended conjugated system.

The minimal transmission for the most promising compound, Zn_CCTMS, reached 50%, which is above the value reported for the previously discussed hemiporphyrazine (~ 30% at 3 $J.cm^{-2}$) acting through a similar mechanism. We surmise that 5,10-A_2B_2 compounds would exhibit better OL efficiency if probed at shorter wavelengths for NLA. The experimental wavelength of 532 nm was situated in close vicinity to the Q-bands area for the 5,10-A_2B_2 porphyrins studied. Both singlet and triplet excited state absorption cross-sections were reported to reach their maxima between the Soret and Q-bands for porphyrins. In the close vicinity to the Q-band area both absorption cross-sections are lower.[27] Possibly weak ESA at 532 nm lowers the overall transmission drop detected for the 5,10-A_2B_2 porphyrins studied.

Compound Pd_Br, for which the Q-band maximum was equal to the experimental wavelength of 532 nm, exhibited a linear absorption approximately 1.5 to 5 times higher at that wavelength compared to other compounds. Evidently, the excited state cross-section was lower than that of the ground state ($\kappa_1 < 1$) for this compound, both in toluene and in DMF, resulting in SA observed at lower fluences. The SA/RSA/SA character of the response developed in the two solvents. Yet, SA/RSA and RSA/SA

turnover fluences and the magnitude of transmission rise and drop (thought SA and subsequent RSA before final SA occurred) differed significantly between the two solvent. The values of parameters (model **E,** Table 1), were much more different for the two solvents for compound Pd_Br in reference to other compounds, for which the values of parameters appeared to be of the same order of magnitude for the two solvents.

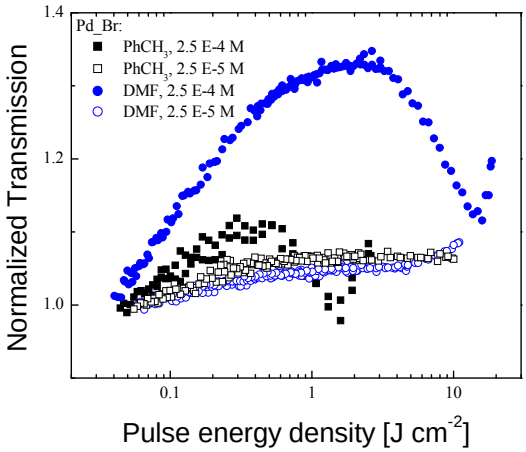

Figure 14: Nonlinear absorption responses of compound Pd_Br recorded in toluene and DMF at different molar concentrations.

Srinivas *et al.* observed that NLA response of Rhodamine B in the ps regime changed from SA to SA/RSA when the concentration was increased, which was associated with aggregation.[17] Konstantaki *et al.* observed some similar phenomena for osmium complexes in the ns regime. Although the SA/RSA character of the response was maintained for different concentrations the threshold intensity for RSA was slightly lower at higher concentration. The RSA character of the response was attributed to charge transfer processes occurring in highly excited states.[16] We measured the NLA response of diluted samples of compound Pd_Br in DMF and toluene and noticed that a switch to RSA was no longer detectable, which is in agreement with the previous reports. As illustrated in Fig. 14, diluted

samples of compound Pd_Br in both solvents exhibited weak and comparable SA. Responses at higher concentration varied much more that those at lower concentrations implying, aggregation to occur in one of the solvents. Self-aggregation of metalloporphyrins is a well known phenomenon.[35] Previous reports showed that electron-withdrawing substituents on the molecule's periphery enhance π-π stacking.[36] Therefore, aggregation may be expected for compound Pd_Br. Generally, aggregation adds relaxation pathways, resulting in shorter lifetimes of the excited states. It also lowers the yield of triplet state formation.[37, 38] Our preliminary UV-vis studies, which we do not present herein, showed that Pd_Br forms aggregates in DMF to concentration of up to 10^{-4} M. (No such behavior was observed for other compounds studied in DMF or in toluene.) The model applied assumes that ISC process is quick and efficient. Yet, one can deduce how a lower yield of triplet state formation impacts on the fitting parameters. A lower yield of triplet state formation will lower the population of the state N_1. Thus, higher intensities will be needed to populate efficiently N_1 so that significant one-photon ESA could arise from it. Therefore, one can expect that higher intensities will be needed to saturate the one-photon process. Additionally, shorter lifetimes of the excited states should enhance the saturation intensities. It can be observed that both I_2 and I_3 are two orders of magnitude larger in DMF than in toluene.

Conclusions

The NLA properties of 5,10-A_2B_2 porphyrins were investigated with the open Z-scan technique in toluene and DMF. The responses were found to be dependent on structural features, the solvent used and the input fluence. Although the character of the responses varied between compounds, the same model was shown to be suitable to follow the evolution of NLA with input fluence for all of the compounds. A four-level model, where one-photon ESA is followed by a simultaneous TPA process arising from the higher excited state was proposed to explain the NLA in 5,10-A_2B_2 porphyrins. This indicated that all 5,10-A_2B_2 compounds share similar excited state structures and that the specific 5,10-

A_2B_2 regiochemical substitution pattern results in a NLA behavior distinct from that found in meso tetrasubstituted compounds, where NLA is typically explained by one-photon ESA. The steady state model approximated the NLA processes arising in 5,10-A_2B_2 porphyrins well. We found the stability of the signal to be depended on the solvent; reproducible data could be obtained at much higher intensities in DMF in comparison to toluene. For all compounds which exhibited an overall transmission drop with intensity (Zn_Br, 2H_CCTMS and Pd_CCTMS) the minimal transmission reached a lower value in toluene than in DMF. Higher ratios of the excited to ground state absorption cross-sections were obtained in toluene than in DMF. Zn complex with TMS-ethynyl groups Zn_CCTMS tuned out to be most promising candidate for OL application. Compound Pd_Br with strong linear absorption at the experimental wavelength exhibited a SA/RSA/SA response in both solvents. The fitting parameters differed much more between the two solvent studied compared to other compounds. This was associated with enhanced aggregation of this compound in DMF. Clearly, these initial studies on 5,10-A_2B_2 porphyrins reveal interesting NLA properties which will be investigated further.

Appendix

N_i stands for the populations densities corresponding to *i*-th electronic state, τ_i - for excited state lifetime, σ_i – ground (i = 0) and excited states (i >0) absorption cross-sections, N is the total population density and α_0 is the linear absorption coefficient. The latter two parameters are correlated according to:

$$\alpha_0 = N\sigma_0 \qquad \text{(Eq. A4)}$$

The populations of the highest excited states are neglected in all models. Steady state approximation is applied, *i.e.* $dN_i/dt = 0$.

Model **A**

$$\frac{dN_0}{dt} = -\frac{N_0\sigma_0 I}{h\nu} + \frac{N_1}{\tau_1} \quad \text{(Eq. A5)}$$

$$\frac{dN_1}{dt} = \frac{N_0\sigma_0 I}{h\nu} - \frac{N_1}{\tau_1} \quad \text{(Eq. A6)}$$

$$\frac{dI}{dz'} = -\sigma_0 N_0 I - \sigma_1 N_1 I \quad \text{(Eq. A7)}$$

$$N = N_0 + N_1 \quad \text{(Eq. A8)}$$

Defining:

$$I_1 = \frac{h\nu}{\sigma_0\tau_1} \quad \text{(Eq. A9)}$$

$$\kappa_1 = \frac{\sigma_1}{\sigma_0} \quad \text{(Eq. A10)}$$

and after some formula rearrangements, the expression for *α(I)* takes the following form:

$$\alpha(I) = \alpha_0 \frac{1+\kappa_1\frac{I}{I_1}}{1+\frac{I}{I_1}} \quad \text{(Eq. A11)}$$

Model **B**[9, 14, 39]

Eq. A5

$$\frac{dN_1}{dt} = \frac{N_0\sigma_0 I}{h\nu} - \frac{N_1}{\tau_1} - \frac{N_1\sigma_1 I}{h\nu} + \frac{N_2}{\tau_2} \quad \text{(Eq. 12)}$$

$$\frac{dN_2}{dt} = \frac{N_1\sigma_1 I}{h\nu} - \frac{N_2}{\tau_2} \quad \text{(Eq. A13)}$$

$$\frac{dI}{dz\prime} = -\sigma_0 N_0 I - \sigma_1 N_1 I - \sigma_2 N_2 I \quad \text{(Eq. A14)}$$

$$N = N_0 + N_1 + N_2 \quad \text{(Eq. A15)}$$

Defining:

$$I_2 = \frac{h\nu}{\sigma_1\tau_2} \quad \text{(Eq. A16)}$$

$$\kappa_2 = \frac{\sigma_2}{\sigma_0} \quad \text{(Eq. A17)}$$

I_1 and κ_1 as defined before according to Eq. A9 and Eq. A10, respectively. After some formula rearrangements, the expression for *α(I)* takes the following form:

$$\alpha(I) = \alpha_0 \frac{1+\kappa_1\frac{I}{I_1}+\kappa_2\frac{I^2}{I_1 I_2}}{1+\frac{I}{I_1}+\frac{I^2}{I_1 I_2}} \qquad \text{(Eq. A18)}$$

Model **C**

Eq. A5, Eq. A12

$$\frac{dN_2}{dt} = \frac{N_1\sigma_1 I}{h\nu} - \frac{N_2}{\tau_2} - \frac{N_2\sigma_2 I}{h\nu} + \frac{N_3}{\tau_3} \qquad \text{(Eq. A19)}$$

$$\frac{dN_3}{dt} = \frac{N_2\sigma_2 I}{h\nu} - \frac{N_3}{\tau_3} \qquad \text{Eq. A20)}$$

$$\frac{dI}{dz'} = -\sigma_0 N_0 I - \sigma_1 N_1 I - \sigma_2 N_2 I - \sigma_3 N_3 I \quad \text{(Eq. A21)}$$

$$N = N_0 + N_1 + N_2 + N_3 \qquad \text{(Eq. A22)}$$

Defining:

$$I_3 = \frac{h\nu}{\sigma_2\tau_3} \qquad \text{(Eq. A23)}$$

$$\kappa_3 = \frac{\sigma_3}{\sigma_0} \qquad \text{(Eq. A24)}$$

I_1, I_2, κ_1 and κ_2 as defined before according to Eq. A9, Eq. A16, Eq. A10 and Eq. A17, respectively. After some formula rearrangements, the expression for $\alpha(I)$ takes the following form:

$$\alpha(I) = \alpha_0 \frac{1+\kappa_1\frac{I}{I_1}+\kappa_2\frac{I^2}{I_1 I_2}+\kappa_3\frac{I^3}{I_1 I_2 I_3}}{1+\frac{I}{I_1}+\frac{I^2}{I_1 I_2}+\frac{I^3}{I_1 I_2 I_3}} \qquad \text{(Eq. A25)}$$

Model **D**

Eq. A5, Eq. A12, A13 and Eq. A15

$$\frac{dI}{dz'} = -\sigma_0 N_0 I - \sigma_1 N_1 I - \sigma_2 N_2 I^2 \qquad \text{(Eq. 26)}$$

I_1, I_2, κ_1 and κ_2 as defined before according to Eq. A9, Eq. A16, Eq. A10 and Eq. A17, respectively. After some formula rearrangements, the expression for $\alpha(I)$ takes the following form:

$$\alpha(I) = \alpha_0 \frac{1+\kappa_1\frac{I}{I_1}+\kappa_2\frac{I^3}{I_1 I_2}}{1+\frac{I}{I_1}+\frac{I^2}{I_1 I_2}} \qquad \text{(Eq. A27)}$$

Model **E**

Eq. A5, Eq. A12 and A22.

$$\frac{dN_2}{dt} = \frac{N_1\sigma_1 I}{h\nu} - \frac{N_2}{\tau_2} - \frac{N_2\sigma_2 I^2}{2h\nu} + \frac{N_3}{\tau_3} \qquad \text{(Eq. 28)}$$

$$\frac{dN_3}{dt} = \frac{N_2\sigma_2 I^2}{2h\nu} - \frac{N_3}{\tau_3} \qquad \text{(Eq. A29)}$$

Defining:

$$I_3 = \frac{2h\nu}{\sigma_2\tau_3} \qquad \text{(Eq, A30)}$$

$$\kappa_3 = \frac{\sigma_3}{\sigma_0} \qquad \text{(Eq. A31)}$$

I_1, I_2, κ_1 and κ_2 as defined before according to Eq. A9, Eq. A16, Eq. A10 and Eq. A17, respectively. After some formula rearrangements, the expression for $\alpha(I)$ takes the following form:

$$\alpha(I) = \alpha_0 \frac{1+\kappa_1\frac{I}{I_1}+\kappa_2\frac{I^3}{I_1 I_2}+\kappa_3\frac{I^4}{I_1 I_2 I_3}}{1+\frac{I}{I_1}+\frac{I^2}{I_1 I_2}+\frac{I^4}{I_1 I_2 I_3}} \qquad \text{(Eq. A32)}$$

Acknowledgements

This work was supported by a grant from Science Foundation Ireland (SFI P.I. 09/IN.1/B2650). J.W. received financial support from the 100-Talent Program of the Chinese Academy of Sciences, the National Natural Science Foundation of China (NSFC, Grant No. 61178007), and the Science and Technology Commission of Shanghai Municipality (STCSM Nano Project, Grant No. 11nm0502400).

(1) Senge, M. O.; Fazekas, M.; Notaras, E. G. A.; Blau, W. J.; Zawadzka, M.; Locos, O. B.; Mhuircheartaigh, E. M. N. *Adv. Mater.* **2007**, *19*, 2737-2774.

(2) Sun, Y. P.; Riggs, J. E. *Int. Rev. Phys. Chem.* **1999**, *18*, 43-90.

(3) Tutt, L. W.; Boggess, T. F. *Prog. Quant. Electr.* **1993**, *17*, 299-338.

(4) Jablonski, A. *Nature*, **1933**, *131*, 839-840.

(5) Mishra, S. R.; Mehendale, S. C. In *Handbook of Advanced Electronic and Photonic Materials and Devices: Nonlinear optical materials*; Nalwa, H. S., Ed.; Academic Press: San Diego, 2001.

(6) Si, J. H.; Yang, M.; Wang, Y. X.; Zhang, L.; Li, C. F.; Wang, D. Y.; Dong, S. M.; Sun, W. F. *Appl. Phys. Lett.* **1994**, *64*, 3083-3085.

(7) Swatton, S. N. R.; Welford, K. R.; Till, S. J.; Sambles, J. R. *Appl. Phys. Lett.* **1995**, *66*, 1868-1870.

(8) Przhonska, O. V.; Lim, J. H.; Hagan, D. J.; Van Stryland, E. W.; Bondar, W. V.; Slominsky, Y. L. *J. Opt. Soc. Am. B: Opt. Phys.* **1998**, *15*, 802-809.

(9) Kiran, P. P.; Reddy, D. R.; Maiya, B. G.; Dharmadhikari, A. K.; Kumar, G. R.; Desai, N. R. *Appl. Opt.* **2002**, *41*, 7631-7636.

(10) Deng, X. X.; Zhang, X. R.; Wang, Y. X.; Song, Y. L.; Liu, S. T.; Li, C. F. *Opt. Commun.* **1999**, *168*, 207-212.

(11) Notaras, E. G. A.; Fazekas, M.; Doyle, J. J.; Blau, W. J.; Senge, M. O. *Chem. Commun.* **2007**, 2166-2168.

(12) Srinivas, N.; Rao, S. V.; Rao, D.; Kimball, B. K.; Nakashima, M.; Decristofano, B. S.; Rao, D. N. *J. Porphyrins Phthalocyanines* **2001**, *5*, 549-554.

(13) Dini, D.; Vagin, S.; Hanack, M.; Amendola, V.; Meneghetti, M. *Chem. Commun.* **2005**, 3796-3798.

(14) Gao, Y.; Chang, Q.; Ye, H.; Jiao, W.; Song, Y.; Wang, Y.; Qin, J. *Appl. Phys. B: Lasers Opt.* **2007**, *88*, 255-258.

(15) George, M.; Muneera, C. I.; Singh, C. P.; Bindra, K. S.; Oak, S. M. *Opt. Laser Technol.* **2008**, *40*, 373-378.

(16) Konstantaki, M.; Koudoumas, E.; Couris, S.; Laine, P.; Amouyal, E.; Leach, S. *J. Phys. Chem. B* **2001**, *105*, 10797-10804.

(17) Srinivas, N.; Rao, S. V.; Rao, D. N. *J. Opt. Soc. Am. B* **2003**, *20*, 2470-2479.

(18) Kiran, P. P.; Reddy, D. R.; Dharmadhikari, A. K.; Maiya, B. G.; Kumar, G. R.; Rao, D. N. *Chem. Phys. Lett.* **2006**, *418*, 442-447.

(19) Dini, D.; Calvete, M. J. F.; Hanack, M.; Amendola, V.; Meneghetti, M. *J. Am. Chem. Soc.* **2008**, *130*, 12290-12298.

(20) Calvete, M.; Yang, G. Y.; Hanack, M. *Synth. Met.* **2004**, *141*, 231-243.

(21) Senge, M. O.; Ryppa, C.; Fazekas, M.; Zawadzka, M.; Dahms, K. *Chem. Eur. J.* **2011**, *17*, 13562-13573.

(22) Senge, M. O.; Shaker, Y. M.; Pintea, M.; Ryppa, C.; Hatscher, S. S.; Ryan, A.; Sergeeva, Y. *Eur. J. Org. Chem.* **2010**, 237-258.

(23) Sheikbahae, M.; Said, A. A.; Wei, T. H.; Hagan, D. J.; Vanstryland, E. W. *IEEE J. Quantum Electron.* **1990**, *26*, 760-769.

(24) Milgrom, R. L. *The colours of life: an introduction to the chemistry of porphyrins and related compounds*, Oxford University Press: New York, 1997.

(25) Kimball, B. R.; Nakashima, M.; DeCristofano, B. S. *SPIE Proceed.* **2000**, *4106*, 264-271.

(26) Koudoumas, E.; Ruth, A. A.; Couris, S.; Leach, S. *Mol. Phys.* **1996**, *88*, 125-133.

(27) McEwan, K. J.; Bourhill, G.; Robertson, J. M.; Anderson, H. L. *J. Nonlinear Opt. Phys. Mater.* **2000**, *9*, 451-468.

(28) a) Azenha, E. G.; Serra, A. C.; Pineiro, M.; Pereira, M. M.; de Melo, J. S.; Arnaut, L. G.; Formosinho, S. J.; Gonsalves, A. *Chem. Phys.* **2002**, *280*, 177-190; b) Bonnett, R. *J. Chem. Soc. Farady Trans.* **1992,** *88(6),* 763-769.

(29) Venkatram, N.; Rao, D. N.; Giribabu, L.; Rao, S. V. *Appl. Phys. B: Lasers Opt.* **2008**, *91*, 149-156.

(30) O'Flaherty, S. M.; Hold, S. V.; Cook, M. J.; Torres, T.; Chen, Y.; Hanack, M.; Blau, W. J. *Adv. Mater.* **2003**, *15*, 19-32.

(31) Duarte, F. J.; Hillman, L. W. *Dye laser principles : with applications*, Academic Press: Boston, 1990.

(32) Röder, B.; Büchner, M.; Rückmann, I.; Senge, M. O. *Photochem. Photobiol. Sci.* **2010**, *9*, 1152-1158.

(33) Rao, D. N. *Opt. Mater.* **2003**, *21*, 45-49.

(34) Zawadzka, M.; Wang, J.; Blau, W. J.; Senge, M. O. *Chem. Phys. Lett.* **2009**, *477*, 330-335.

(35) White, W. I. In *The porphyrins*; Dolphin, D., Ed.; Academic Press: New York, 1978.

(36) Abraham, R. J.; Eivazi, F.; Pearson, H.; Smith, K. M. *J. Chem. Soc., Chem. Commun.* **1976**, 699-701.

(37) Barzda, V.; Peterman, E. J. G.; van Grondelle, R.; van Amerongen, H. *Biochemistry* **1998**, *37*, 546-551.

(38) Damoiseau, X.; Tfibel, F.; Hoebeke, M.; Fontaine-Aupart, M. P. *Photochem. Photobiol.* **2002**, *76*, 480-485.

(39) Gao, Y. C.; Zhang, X. R.; Li, Y. L.; Liu, H. F.; Wang, Y. X.; Chang, Q.; Jiao, W. Y.; Song, Y. L. *Opt. Commun.* **2005**, *251*, 429-433.

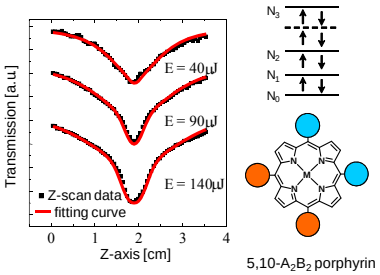

5,10-A_2B_2 porphyrin